THE JOURNAL OF BIOLOGICAL CHEMISTRY VOL. 285, NO. 26, pp. 20399–20409, June 25, 2010

Basis for the Specificity and Activation of the Serpin Protein Z-dependent Proteinase Inhibitor (ZPI) as an Inhibitor of Membrane-associated Factor Xa*[S]

Received for publication, February 9, 2010, and in revised form, April 2, 2010 Published, JBC Papers in Press, April 28, 2010, DOI 10.1074/jbc.M110.112748

Xin Huang[‡1], **Alexey Dementiev**[§1], **Steven T. Olson**[‡¶2], **and Peter G. W. Gettins**[‡§¶3]

From the [‡]*Center for Molecular Biology of Oral Diseases,* [§]*Department of Biochemistry and Molecular Genetics, and* [¶]*Center for Structural Biology, University of Illinois at Chicago, Chicago, Illinois 60607*

The serpin ZPI is a protein Z (PZ)-dependent specific inhibitor of membrane-associated factor Xa (fXa) despite having an unfavorable P1 Tyr. PZ accelerates the inhibition reaction ~2000-fold in the presence of phospholipid and Ca^{2+}. To elucidate the role of PZ, we determined the x-ray structure of Gla-domainless PZ ($PZ_{\Delta GD}$) complexed with protein Z-dependent proteinase inhibitor (ZPI). The PZ pseudocatalytic domain bound ZPI at a novel site through ionic and polar interactions. Mutation of four ZPI contact residues eliminated PZ binding and membrane-dependent PZ acceleration of fXa inhibition. Modeling of the ternary Michaelis complex implicated ZPI residues Glu-313 and Glu-383 in fXa binding. Mutagenesis established that only Glu-313 is important, contributing ~5–10-fold to rate acceleration of fXa and fXIa inhibition. Limited conformational change in ZPI resulted from PZ binding, which contributed only ~2-fold to rate enhancement. Instead, template bridging from membrane association, together with previously demonstrated interaction of the fXa and ZPI Gla domains, resulted in an additional ~1000-fold rate enhancement. To understand why ZPI has P1 tyrosine, we examined a P1 Arg variant. This reacted at a diffusion-limited rate with fXa, even without PZ, and predominantly as substrate, reflecting both rapid acylation and deacylation. P1 tyrosine thus ensures that reaction with fXa or most other arginine-specific proteinases is insignificant unless PZ binds and localizes ZPI and fXa on the membrane, where the combined effects of Gla-Gla interaction, template bridging, and interaction of fXa with Glu-313 overcome the unfavorability of P1 Tyr and ensure a high rate of reaction as an inhibitor.

Blood coagulation is a complex process requiring tight regulation through the use of feedback loops and the involvement of proteinase-specific inhibitors (1). fXa,[4] in complex with its cofactor Va, plays a crucial role in blood coagulation, being directly involved in the generation of the final proteinase thrombin from its zymogen prothrombin. This reaction takes place on the membrane surface of activated platelets, with all three protein components interacting with the membrane surface, either through Gla domains in the case of fXa and prothrombin or the two C-type domains of factor Va. In addition, fXa is itself formed at the membrane surface through the action of factor IXa, in complex with its cofactor VIIIa, on factor X.

To help prevent clot formation away from the site of injury, any fXa that dissociates from the membrane and diffuses away in the bloodstream must be efficiently inhibited. This is accomplished primarily by the serpin antithrombin, which, when allosterically activated by being bound to heparan sulfate chains on the surface of endothelial cells, is a rapid inactivator of fXa, as well as of other circulating arginine-specific proteinases, such as thrombin and factor IXa (2). The P1 residue[5] of antithrombin is arginine, in keeping with the substrate specificity of each of these proteinases. Interestingly, there is a second serpin, ZPI, that specifically inhibits fXa, as well as fXIa (3, 4). However, ZPI requires a protein cofactor, protein Z, and the presence of phospholipid and Ca^{2+} for rapid inactivation of fXa (5). Paradoxically, given the trypsin-like specificity of fXa, ZPI has a P1 tyrosine. Although its cofactor requirements suggest that ZPI may serve a complementary role to antithrombin, as an inhibitor of membrane-associated rather than solution phase fXa, it raises important questions as to what roles the protein cofactor and membrane surface play and, crucially, why the P1 residue of ZPI is not arginine, as is found in antithrombin.

We present here the structure of ZPI in complex with Gla domainless-protein Z ($PZ_{\Delta GD}$), together with a model of the ternary complex with fXa that corresponds to the Michaelis complex. Mutagenesis experiments established the importance of charged and polar residues in the interface between PZ and ZPI for the binding interaction and for Glu-313 in strand 2C of ZPI for interaction with fXa and fXIa. Whereas PZ was found to induce long range conformational changes in ZPI, these were of

* This work was supported, in whole or in part, by National Institutes of Health Grants HL49234 and HL79430 (to P. G. W. G.) and HL78827 (to S. T. O.). This work was also supported by American Heart Association Fellowship 0920029G (to X. H.).

[S] The on-line version of this article (available at http://www.jbc.org) contains supplemental Table 1.

The atomic coordinates and structure factors (code 3H5C) have been deposited in the Protein Data Bank, Research Collaboratory for Structural Bioinformatics, Rutgers University, New Brunswick, NJ (http://www.rcsb.org/).

[1] Both authors contributed equally to this work.

[2] To whom correspondence may be addressed. Tel.: 312-996-1043; E-mail: stolson@uic.edu.

[3] To whom correspondence may be addressed. Tel.: 312-996-5534; E-mail: pgettins@uic.edu.

[4] The abbreviations used are: fXa, factor Xa; fXIa, factor XIa; NBD, 7-nitrobenz-2-oxa-1,3-diazole; PZ, protein Z; $PZ_{\Delta GD}$, protein Z lacking the N-terminal Gla domain; RCL, reactive center loop; SI, stoichiometry of inhibition; ZPI, protein Z-dependent proteinase inhibitor; Bistris propane, 1,3-bis[tris(hydroxymethyl)methylamino]propane; SUV, small unilamellar vesicle; EGF, epidermal growth factor.

[5] P1, P2, etc. follow the nomenclature of Schechter and Berger (38), which designates the scissile bond of a proteinase substrate as P1-P1′.

minor importance for accelerating the rate of inhibition of fXa. Instead, the template-bridging effect of the membrane binding to the Gla domains of both fXa and PZ, together with the specific interaction of the two Gla domains shown previously by Rezaie and co-workers (6), were the most important factors in bringing about the PZ-dependent acceleration of fXa inhibition in the presence of phospholipid and Ca^{2+}. Importantly, we found that a ZPI variant with P1 arginine reacted at a diffusion-limited rate with fXa. Reaction was predominantly as a substrate, as a result of rapid acylation and deacylation, and did not depend on PZ or other cofactors. Thus, although the P1 tyrosine results in a reaction that is several orders of magnitude slower than with P1 arginine, it ensures that reaction of ZPI with fXa only occurs at a significant rate, and as an inhibitor, when ZPI is membrane-associated through complexation with PZ. This is thus another example of deliberate repression of a reaction unless compensating factors that ensure specificity (here for membrane-associated fXa) are present.

EXPERIMENTAL PROCEDURES

Materials—Materials were obtained as follows: SDS, Hepes, Trizma base, EDTA, and polyethylene glycol (M_r, 8,000 and 20,000) from Sigma; prestained molecular weight standards from Bio-Rad; human fXa (fXa), human protein Z and human fXIa from Enzyme Research Laboratories (South Bend, IN); S2366 from Diapharma (West Chester, OH); spectrozyme fXa from American Diagnostica (Greenwich, CT); the fXa fluorogenic substrate, Pefafluor fXa, from Centerchem (Norwalk, CT); the fXIa fluorogenic substrate *t*-butoxycarbonyl-Glu-(OBzl)-Ala-Arg-aminomethylcoumarin from Bachem; and Mono-S HR 5/5, Sephacryl S-200, and SP-Sepharose resins from GE Healthcare. Thrombin was activated from prothrombin isolated from citrated plasma as described previously (7). Recombinant Gla-domainless fXa was a generous gift from Dr. Ray Rezaie (8).

Protein Expression, Isolation, and Purification—ZPI cDNA, including the N-terminal leader sequence, was cloned into the BamHI and EcoRI sites of pFastbac1 vector, and recombinant ZPI was expressed in baculovirus-infected insects cells using the Bac-to-Bac baculovirus expression system (Invitrogen), as in previous studies (9). For the Y387R ZPI variant, E64 was included in the insect cell medium at 5 μg/ml and in buffers used for the initial purification step at 50 μg/ml to minimize the formation of cleaved inhibitor. Single cysteine ZPI variants were prepared by mutation of one of two original cysteines (C169A and C264S) or by introducing new cysteines at positions Leu-381 (P7) or Ser-122 (helix D), with both original cysteines already mutated (C169A and C264S). Other ZPI variants, including the single variants E313A, E383A, and Y387R, the double variant E313A/E383A, and the quadruple variant D74A/D238A/K239A/D293A, were produced with the two wild-type cysteines mutated in the same way. DNA mutagenesis was carried out by PCR, employing the Quick Exchange kit from Stratagene. All mutations were confirmed by DNA sequencing. All ZPI proteins were purified by successive SP-Sepharose, Mono S, and Sephacryl S200 chromatography steps, as in previous studies (9). Cleaved ZPI produced during the expression of the Y387R variant was separated from native ZPI during Mono S chromatography by judicious pooling of fractions based on SDS-PAGE analysis. Wild-type and variant ZPIs were judged >95% pure by SDS-PAGE analysis. The molar concentrations of ZPI and PZ were calculated from the absorbance at 280 nm using molar absorption coefficients of 31,525 and 74,400 M^{-1} cm^{-1}, respectively. The former value was calculated as described previously (10), and the latter value was measured directly (11), using molecular weights of 48,462 and 62,000 respectively.

$PZ_{\Delta GD}$ Preparation—$PZ_{\Delta GD}$ was produced by thrombin cleavage as described earlier (3). Briefly, the reaction was performed at 37 °C for 3 h at an enzyme/substrate ratio of 1:25 (w/w) in 50 mM Tris-HCl buffer, pH 7.5, 0.1 M NaCl, followed by addition of D-Phe-Pro-Arg-chloromethyl-ketone (Sigma) to inhibit enzymatic activity. The cleaved protein was applied to a Q-Sepharose column (Amersham Biosciences), and the pure $PZ_{\Delta GD}$ was eluted by a 25 mM to 1 M NaCl gradient in the same buffer. Thrombin under these conditions cleaved PZ after Arg-43 (3). The concentration of $PZ_{\Delta GD}$ was determined from the absorbance at 280 nm using a calculated molar extinction coefficient of 53,200 M^{-1} cm^{-1}, based on a molecular weight of 56,000.

Binary Complex Formation and Purification—$PZ_{\Delta GD}$ and ZPI were mixed in a 1:1 molar ratio at pH 7.5 in 25 mM Tris-HCl buffer, 150 mM NaCl. The complex was purified on a Superdex 200 column (GE Healthcare) equilibrated with the same buffer system. The eluted complex was concentrated to 11 mg/ml in 10 mM Tris-HCl buffer, pH 7.5, 30 mM NaCl.

Crystallization and Data Collection—Hexagonal crystals of the complex (space group $P6_522$) were obtained from sitting drops containing 2 μl of the complex sample (11 mg/ml) and 2 μl of reservoir solution (0.2 M Bistris propane buffer, pH 8.5, containing 45 mM potassium thiocyanate and 15–17% polyethylene glycol 3350). Crystals grew at 18 °C within 10–12 days to an average size of 70 × 70 × 90 μm and were equilibrated against 10% 2-methyl-2,4-pentanediol (Hampton Research) before they were flash-frozen. Diffraction data were collected at 100 K from a single crystal on a Mar CCD-300 detector at SER-CAT beamline (Advanced Proton Source, Argonne National Laboratory). Data were indexed and processed with the XDS package. The crystal diffracted to 3.3 Å and contained one complex per asymmetric unit (supplemental Table 1). The structure of the complex was solved by molecular replacement using PHASER (CCP4 package) (12) with the structures of native α_1PI (Protein Data Bank entry 1OPH) and human fXa, consisting of residues 28–163 (Protein Data Bank entry 1HCG), as search models. The final model of the complex was obtained by carrying out multiple cycles of refinement consisting of manual model building using Coot (CCP4 package), followed by torsion annealing and energy minimization with REFMAC (CCP4 package) (13). Crystallographic statistics are given in supplemental Table 1. The coordinates have been deposited with the Protein Data Bank, with accession code 3H5C.

Experimental Conditions—All solution phase experiments were conducted in 50 mM Hepes buffer, pH 7.4, containing 0.1 M NaCl, and 0.1% PEG 8000 unless specified otherwise.

Phospholipid Preparation—Inhibition kinetics and stoichiometry experiments with ZPI, PZ, and fXa employed synthetic

phospholipid vesicles consisting of a mixture of 70% dioleoylphosphatidylcholine and 30% dioleoylphosphatidylserine (Avanti Polar Lipids, Alabaster, AL) that were prepared as described previously (14). Binding experiments were done with small unilamellar vesicles (SUVs) of phospholipid containing a molar ratio of 80% dioleoylphosphatidylcholine and 20% dioleoylphosphatidylserine that were prepared as described previously (15). Phospholipid concentration was determined by colorimetric assay based on complex formation with ammonium ferrothiocyanate using a mixture of dioleoylphosphatidylcholine and dioleoylphosphatidylserine as the standard (16).

Light Scattering—Binding of protein to lipid SUVs was measured from change in scattered light intensity in Hepes buffer containing 5 mM $CaCl_2$. Measurements were made in an SLM8000 spectrofluorometer with excitation at 320 nm and measurement of scattering intensity at right angles at the same wavelength (17). Binding of PZ or PZ·ZPI complex to SUVs was measured by titrating small volumes of a concentrated solution of PZ into 25 μM lipid SUVs (monomer concentration) in buffer in the absence or presence of 1 μM ZPI. Alternatively, ZPI was titrated into a solution of 10 μM SUVs and 0.47 μM PZ. The scattering intensity signal measured after each addition of protein was corrected for the buffer signal and for dilution. Control titrations of ZPI or PZ into buffer were used to correct the scattering signal for protein not bound to lipid. Light scattering changes were converted to changes in relative molecular mass based on the methods and parameters described by Nelsestuen and Lim (18). Changes in relative molecular masses of SUVs due to PZ or PZ·ZPI complex binding to lipid vesicles or those resulting from ZPI binding to PZ complexed with SUVs were fitted by quadratic equilibrium binding equations (9).

Stoichiometries of ZPI Reactions with Proteinases—Fixed concentrations of proteinase (0.1–1 μM fXa or 10–100 nM fXIa) were reacted with increasing concentrations of ZPI, ranging from 3- to 100-fold molar excess in the absence or presence of PZ equimolar with the ZPI concentration, 25 μM phospholipid, and 5 mM $CaCl_2$ in reaction volumes of 25–100 μl. After allowing sufficient time to reach maximal inhibition, based on measured second order association rate constants (~1–10 min), the remaining proteolytic activity was measured by diluting the reaction mixture with 1 ml of 100 μM S2366 for fXIa reactions or 100 μM Spectrozyme fXa for fXa reactions and monitoring the absorbance change at 405 nm. Initial rates of hydrolysis were determined from computer fits of substrate hydrolysis progress curves, by a second order polynomial function as described previously (9). The stoichiometry of inhibition (SI) was determined from the fitted abscissa intercept of a linear plot of residual proteinase activity against molar ratio of inhibitor to proteinase. Factor Xa and factor XIa concentrations represent active site concentrations (19).

Kinetics of ZPI-Proteinase Reactions—Second order rate constants for proteinase inactivation by ZPI were measured under pseudo-first order conditions in which the inhibitor was in large molar excess over the proteinase (at least five times greater than the concentration of ZPI required to fully inhibit proteinase) and in the absence or presence of PZ, lipid, and Ca^{2+} cofactors, as indicated. Progress curves for the time-dependent inhibition of proteinase were measured by discontinuous assays in which reaction mixtures were incubated for different times, and the samples were withdrawn and diluted into either 50 μM Pefafluor fXa containing 10 mM EDTA, for fXa inhibition, or 30 μM *t*-butoxycarbonyl-EAR-aminomethylcoumarin for fXIa inhibition. Initial velocities were determined by fitting progress curves as described above. Observed pseudo-first order rate constants (k_{obs}) were obtained by fitting the loss of proteinase activity by an exponential decay function with a nonzero end point that reflected a minor amount of degraded proteinase more resistant to inhibition (<5%) or a steady-state level of enzyme activity due to a balance between the rates of complex formation and complex dissociation (9). Second order association rate constants (k_a) were obtained from the slopes of fits of the linear dependence of k_{obs} on the ZPI concentration ($[ZPI]_0$) according to the following: $k_{obs} = k_a \times [ZPI]_0 + k_d$, where k_d represents the rate constant for ZPI·proteinase complex dissociation. Corrections of k_a for differing SIs were made by multiplying k_a by SI (20).

Kinetics of Dissociation of ZPI·Proteinase Complexes—First order rate constants for the dissociation of ZPI·proteinase complexes (k_d) were directly measured by continuous assays of the time-dependent appearance of fXa or fXIa activity when preformed complexes were diluted extensively into substrate as described previously (9). ZPI·proteinase complexes were prepared by incubating ~100 nM wild-type or variant ZPI with proteinase at ratios approximating the SIs for 2–20 min. In the case of fXa, complexes were prepared in the presence of the cofactors PZ, equimolar with ZPI, 25 μM phospholipid, and 5 mM $CaCl_2$. Complexes formed with the quadruple ZPI variant omitted cofactors. Aliquots of complexes were diluted 100–2000-fold into 1 ml of pre-warmed (25 °C) 50–100 μM Pefafluor fXa fluorescence substrate in buffer containing 10 mM EDTA or into 100 μM S2366 substrate or 30 μM fXIa fluorescence substrate. Initial rates of complex dissociation (<10% dissociation, except for P1 Arg ZPI variant) were monitored from increases in absorbance or fluorescence for 3–15 min, and dissociation rate constants were obtained by fitting progress curves to a parabolic function (9). Dissociation rate constants for ZPI·fXa complexes formed in the absence of cofactors were found to be unaffected when dissociation was monitored in the presence of cofactors.

Fluorophore Labeling—Single cysteine ZPI variants were labeled with iodoacetamido-*N,N′*-dimethyl-*N*-(acetyl)-*N′*-(7-nitrobenz-3-oxa-1,3-diazol-4-yl)ethylenediamine as described previously (21). The extent of fluorophore labeling was determined from the ratio of NBD absorbance to the protein absorbance at 280 nm after correcting the latter for the contribution of the fluorophore. An extinction coefficient of 25,000 M^{-1} cm^{-1} at 478 nm was used for NBD.

Fluorescence Spectroscopy—Perturbation of the fluorescence of NBD-labeled L381C and S122C ZPI variants by complexation with protein Z was assessed by excitation of ~100 nM NBD-labeled ZPI at 480 nm and measuring the emission spectrum between 500 and 600 nm in 5-nm steps (5–10-s integrations) with an SLM 8000 spectrofluorometer. The effects of interaction with protein Z were determined by titrating with protein Z and monitoring the fluorescence change after each addition. All spectra were recorded at least twice and averaged

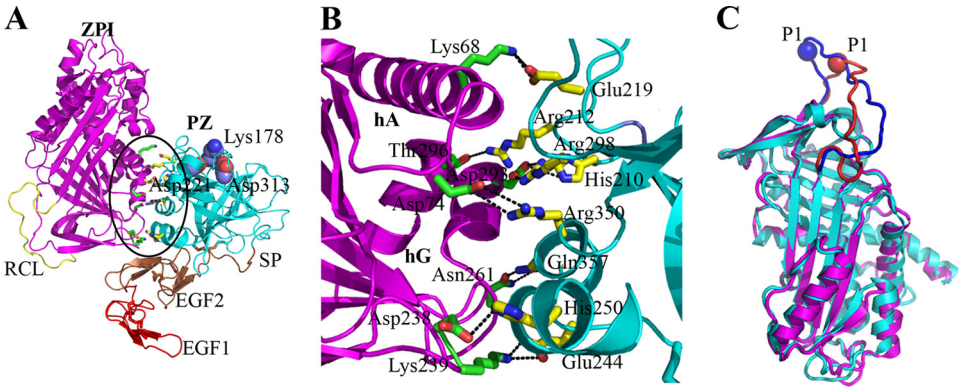

FIGURE 1. **Structure of the binary ZPI·protein Z complex.** *A,* structure of the complex in *ribbon* representation, with ZPI in *pink* and PZ in *blue* (pseudo-catalytic domain, *SP*), *brown* (EGF2 domain), and *red* (EGF1 domain). The RCL is *yellow*. Residues in PZ that would correspond to the catalytic triad in functional serine proteinase domains are shown in space filling (Lys-178, Asp-221, and Asp-313, corresponding to His, Asp, and Ser of the triad, respectively). The contact region between ZPI and PZ is highlighted by an *ellipse*. *B,* close up of the ZPI:PZ contact region, showing the polar and charged interactions that populate the interface. *C,* overlay of ribbon diagram structures of the ZPI moiety from the present complex with $PZ_{\Delta GD}$ (*cyan*) and from an earlier structure of the complex with PZ lacking both Gla and EGF1 domains (*pink*). The structures are almost identical, with the major exception of the orientation of the RCL and hence the position of the P1 residue. This may simply result from packing effects, but it affects any subsequent modeling of the ternary Michaelis complex.

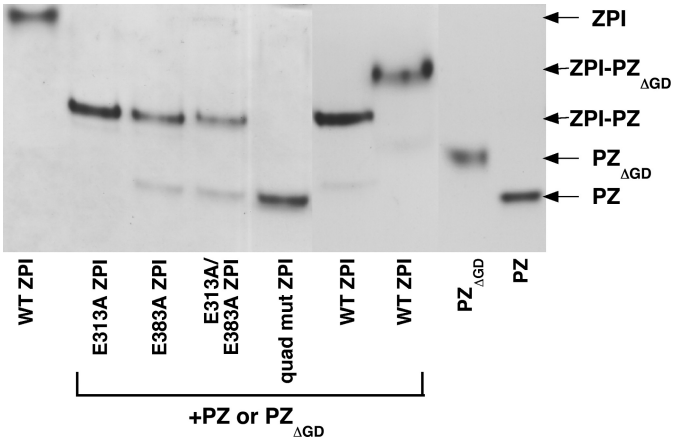

FIGURE 2. **Importance of charged residues at the ZPI:PZ interface.** Comparison of the ability of PZ or $PZ_{\Delta GD}$ to interact with wild-type ZPI or variants E313A, E383A, E313A/E383A, or the quadruple mutant by native PAGE. Although the wild type and variants containing one or both Glu-313 or Glu-383 mutations all form complex with PZ or $PZ_{\Delta GD}$, the interface quadruple variant does not. Note that the free ZPI double or quadruple variants do not migrate into the gel because of the loss of two negative charges.

and were corrected for dilution (<10%) and buffer background. Experiments of each labeled ZPI with PZ or $PZ_{\Delta GD}$ were performed two or more times and the results averaged.

Reaction of Variants with 5-Iodoacetamidofluorescein—Change in exposure of ZPI cysteines as a function of bound protein Z was determined from the rate of reaction of 3 μM ZPI with single cysteines at positions 122, 169, and 381 with 200–400 μM 5-iodoacetamidofluorescein. Rates were determined from quantitation of fluorescein fluorescence associated with the ZPI variant band after PAGE analysis of 4-μg samples of reactions with 5-iodoacetamidofluorescein (22). Bands were visualized by fluorescence, using a UV transilluminator, and photographed. Scanned photographic images were quantitated by densitometry.

PAGE and Immunoblotting—Native PAGE was performed at 4 °C using the Laemmli buffer system with 5.5% gels and running times of 2–5 h at 110–150 V. SDS-PAGE was performed with the same buffer system, but with 10% gels, at room temperature. Protein bands were detected by Coomassie Blue staining.

RESULTS

Structure of the ZPI·$PZ_{\Delta GD}$ Complex—Fig. 1 shows our 3.3 Å resolution structure of the complex between recombinant ZPI and Gla-domainless human plasma PZ. It is more complete than the one published recently in having the pseudo-catalytic domain and both of the EGF domains of protein Z, whereas the EGF1 domain of protein Z was absent from the earlier structure (23). However, the overall structure is similar to the first one in most respects. For the ZPI moiety, the whole of the backbone is visible (Fig. 1*A*), with the exception of the first 39 residues, all of which are part of the N-terminal tail, which is an extension that is not present in other serpins. In addition, one residue of carbohydrate is visible attached to each of Asn-176 and Asn-274. Of the residues of the core serpin fold, side chains can be traced for 339 out of 384. The exceptions are mostly in surface loops, including the linker between strand 3A and helix F and part of the reactive center loop (RCL), including the P1 Tyr. The serpin core shows very high structural similarity to other serpins, including the related A clade member SERPINA1 (α_1PI), with nine α-helices packed against three β-sheets. The root mean square deviation between α_1PI and the corresponding main chain atoms of ZPI is 1.0 Å. Helix A, which is the first visible feature, is 47 Å and nine turns in length. This is two turns longer on the N-terminal end than in α_1PI. As in other serpins, the RCL is prominently exposed at one end of the molecule and adopts an extended β-like conformation, although the proximal hinge region is not inserted into β-sheet A (24). Although the side chains of residues P17 through P4 are mostly well defined, those of P3 to P2′ are not visible, suggesting quite high mobility in this region, which is expected to be part of the fXa-binding site. Given the exposed nature of the RCL and its consequent susceptibility to crystal packing effects, it is perhaps not surprising that this is the one region of ZPI that differs significantly between the current complex structure and the earlier one. Superpositioning of the ZPI molecules from the two complexes reveals minimal differences throughout the body of the serpin but marked difference in conformation and position of the whole loop, including the P1 residue (Fig. 1*C*).

To increase the likelihood of obtaining well diffracting crystals, the protein Z used in this study had the N-terminal Gla domain proteolytically removed, although this did not abrogate its ability to bind to ZPI, based on gel-shift assay (Fig. 2). Of the remaining 317 PZ residues, the backbone of 312, starting two residues before the first Cys of the EGF1 domain (Cys-51), and side chains of 278 can be traced in our structure (Fig. 1*A*). Of the predicted carbohydrate, one sugar residue can be traced at four

TABLE 1

Kinetic constants for ZPI reactions with fXa in the absence and presence of protein Z, lipid, and calcium cofactors

Association rate constants and SIs for ZPI-fXa reactions conducted in the absence of cofactors (k_{uncat}) or in the presence of PZ, phospholipid, and Ca^{2+} cofactors (k_{cat}) and rate constants for ZPI·FXa complex dissociation (k_d) were measured as described under "Experimental Procedures." Association rate constants were corrected for reaction through the substrate pathway by multiplying by the SI (20). I is inhibitor; E is proteinase; ND is not determined.

ZPI	k_{uncat}	SI	$k_{uncat} \times SI$	k_{cat}	SI	$k_{cat} \times SI$	k_d
	$M^{-1}s^{-1}$	*mol I/mol E*	$M^{-1}s^{-1}$	$M^{-1}s^{-1}$	*mol I/mol E*	$M^{-1}s^{-1}$	s^{-1}
Wild type	$1.0 \pm 0.1 \times 10^4$	3.6 ± 0.4	$3.6 \pm 0.8 \times 10^4$	$9.1 \pm 0.2 \times 10^6$	3.1 ± 0.2	$2.8 \pm 0.2 \times 10^7$	$1.8 \pm 0.3 \times 10^{-4}$
E313A	$1.7 \pm 0.1 \times 10^3$	4.5 ± 0.5	$7.7 \pm 1.3 \times 10^3$	$7.8 \pm 0.4 \times 10^5$	3.3 ± 0.3	$2.6 \pm 0.4 \times 10^6$	$1.8 \pm 0.1 \times 10^{-4}$
E383A	$9.8 \pm 0.2 \times 10^3$	7.1 ± 0.4	$7.0 \pm 0.5 \times 10^4$	$4.6 \pm 0.2 \times 10^6$	4.8 ± 0.1	$2.2 \pm 0.1 \times 10^7$	$1.7 \pm 0.5 \times 10^{-4}$
E313A/E383A	$3.1 \pm 0.2 \times 10^2$	11.0 ± 0.5	$3.4 \pm 0.4 \times 10^3$	$5.1 \pm 0.4 \times 10^5$	6.1 ± 0.2	$3.1 \pm 0.3 \times 10^6$	ND
Quad	$5.1 \pm 0.6 \times 10^3$	9.8 ± 0.2	$5.0 \pm 0.7 \times 10^4$	$1.3 \pm 0.1 \times 10^4$	11.0 ± 0.5	$1.4 \pm 0.2 \times 10^5$	$2.0 \pm 0.2 \times 10^{-4}$
P1 Arg	$3.1 \pm 0.2 \times 10^4$	380 ± 30	$1.2 \pm 0.2 \times 10^7$	$9.5 \pm 1.2 \times 10^4$	440 ± 10	$4.2 \pm 0.1 \times 10^7$	$3.2 \pm 0.2 \times 10^{-3}$

of the *N*-linked attachment sites (Asn-59, Asn-185, Asn-193, and Asn-292) and at one of the *O*-linked attachment sites (Ser-53). Both EGF domains are well defined and extend in an arc from one side of the C-terminal domain. This results in a maximum end-to-end separation of the whole molecule of about 74 Å. As expected, the C-terminal 230 residues form a compact domain with a fold like that of trypsin family serine proteinases (25, 26). Disulfides are present at the predicted positions of 131–132, 133–241, 163–179, and 287–301. Also as expected, the residues that substitute for the catalytic His and Ser of functional trypsin family proteinases (here Lys-178 and Asp-313, respectively) in the pseudo-active site are close together, and near the top of the molecule (27) (Fig. 1*A*), with Cα-Cα separation of 8.3 Å, the same as in fXa, although the third residue of the triad is the normal Asp (Asp-221). The replacement for the Asp at the bottom of the P1 specificity pocket of functional arginine-specific proteinases (here Ala-307) is further away from Asp-313 (16.9 Å for Cα-Cα) than the Asp is from the catalytic Ser in fXa (12.1 Å Cα-Cα).

The interface between protein Z and ZPI is as found in the earlier complex and involves ionic and hydrogen bond interactions between Glu-244, His-250, Arg-350, Gln-357, His-210, Arg-298, Arg-212, and Glu-219 from protein Z with Lys-239, Asp-238, Asn-261, Asp-74, Asp-293, Thr-296, and Lys-68 from ZPI (Fig. 1*B*). This interface is on the side of ZPI, well removed from the reactive center loop, and is at the C-terminal end of the long helix A and centered on helix G. Of the seven charged/polar residues on ZPI involved, all are either fully conserved or have appropriate charged/polar replacements in the five other known ZPI sequences (orangutan, chimp, rat, mouse, and chicken).

Importance of Charged Residues at the Protein Z:ZPI Interface—The importance of the charged residues discussed above in maintaining the interface between PZ and ZPI was tested experimentally by creating a ZPI variant with four of the residues changed to alanine (Asp-74, Asp-238, Lys-239, and Asp-293). The quadruple variant was nearly as active as wild-type ZPI in inhibiting both fXa and fXIa in the absence of protein Z, lipid, and Ca^{2+}, but it was not significantly activated by the cofactors for inactivation of fXa (Tables 1 and 2). Similarly, no shift was seen by native PAGE under conditions where both wild-type ZPI and the Glu-313/Glu-383 variants form a complex with PZ (Fig. 2).

To further examine the effects of the quadruple mutation, we used light scattering as a sensitive means of quantitating the association of ZPI with PZ complexed to small unilamellar phosphatidylserine/phosphatidylcholine lipid vesicles (SUVs). Whereas PZ or ZPI alone or ZPI in the presence of SUVs and Ca^{2+} caused minimal scatter, PZ caused a saturable increase in light scattering intensity in the presence of SUVs and Ca^{2+}, consistent with membrane association resulting from the presence of a membrane-binding Gla domain and in agreement with previous studies (17). When both PZ and ZPI were added, a similar saturable increase in scatter was observed, although with a larger change in scattering intensity, reflecting the dependence of scatter on the mass of the protein components and thus resulting from the binding of ZPI to the SUV-bound PZ (Fig. 3*A*). The effect of the quadruple mutations was to abrogate the ability of ZPI to bind to PZ, as indicated by the finding that the variant ZPI produced no detectable increase in light scattering when titrated into lipid-bound PZ, under conditions where wild-type ZPI caused a saturable increase in scattering, reflecting a tight 1:1 stoichiometric interaction with lipid-complexed PZ (Fig. 3*B*).

TABLE 2

Kinetic constants for ZPI reactions with fXIa in the absence of cofactors

I is inhibitor; E is proteinase; ND is not determined.

ZPI	$k_{a,app}$	SI	$k_{a,app} \times SI$	k_d
	$M^{-1}s^{-1}$	*mol I/mol E*	$M^{-1}s^{-1}$	s^{-1}
Wild type	$1.2 \pm 0.1 \times 10^5$	7.9 ± 0.6	$9.5 \pm 1.5 \times 10^5$	$6.2 \pm 1.4 \times 10^{-5}$
E313A	$9.7 \pm 0.3 \times 10^3$	11.4 ± 0.3	$1.1 \pm 0.1 \times 10^5$	ND
E383A	$4.2 \pm 0.3 \times 10^4$	13.9 ± 0.1	$5.8 \pm 0.5 \times 10^5$	ND
E313A/E383A	$4.8 \pm 0.6 \times 10^3$	20.1 ± 0.2	$9.6 \pm 1.3 \times 10^4$	ND
Quad	$4.9 \pm 0.2 \times 10^4$	15.8 ± 0.2	$7.7 \pm 0.4 \times 10^5$	ND
P1 Arg	$5.6 \pm 0.7 \times 10^3$	1100 ± 400	$6.2 \pm 3.0 \times 10^6$	$2.2 \pm 0.4 \times 10^{-3}$

Ternary Michaelis Complex of fXa·ZPI·Protein Z—A model of the ternary Michaelis complex of fXa with ZPI·protein Z was made by docking fXa with the RCL of ZPI in our binary ZPI·protein Z complex (Fig. 4*A*). The orientation of fXa relative to the RCL of ZPI was based on that of proteinase and serpin in the binary Michaelis complex of α_1PI Pittsburgh with S195A trypsin. In that structure, the RCL of α_1PI has an extended canonical β-like conformation, as here for ZPI, allowing residues P2 to P2′ to interact with the proteinase without any change in conformation being necessary. With this orientation, and with the P1 residue docked into the active site of fXa, there was a striking additional interaction between the charged guanidinium moiety of Arg-143 from fXa (Fig. 4*B*), which has already been identified as important for binding to ZPI (28), with the side chains of both Glu-383 and Glu-313. Glu-383 is in the RCL at P5, and Glu-313 is in the underlying strand 2 of sheet C. This suggested a potentially important

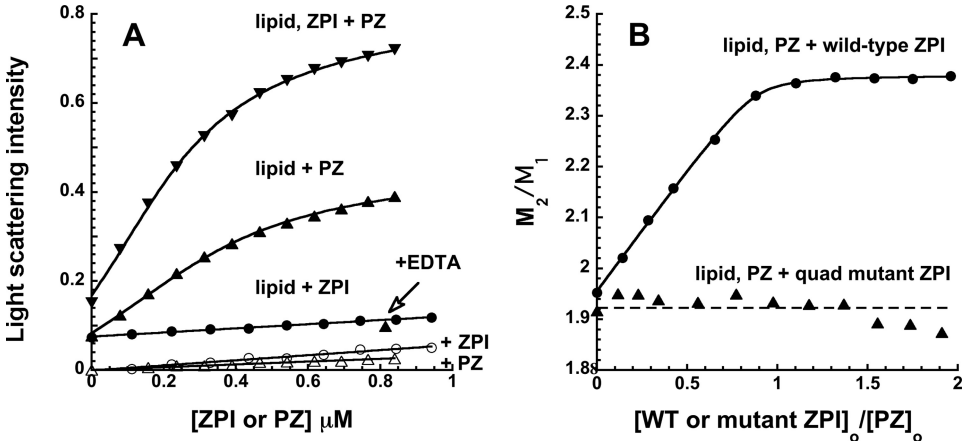

FIGURE 3. **Interaction of PZ, ZPI, and PZ·ZPI complexes with SUVs.** Changes in light scattering resulting from addition of ZPI and/or PZ to SUVs under various conditions. *A,* PZ added to SUVs (25 μM lipid monomer) alone (▲) or in the presence of 1 μM ZPI (▼). ZPI was added to SUVs (25 μM lipid monomer) (●). Controls of PZ (△) and ZPI (○) were titrated without lipid. Also shown is the effect of adding EDTA to the lipid·PZ complex. *Solid lines* are fits of PZ or PZ:ZPI binding data by the quadratic equilibrium binding equation plus a linear term to account for scattering due to free protein. K_D values of ~0.1 μM and 70–90 sites/SUV were obtained from these fits. *B,* changes in the relative molecular mass (M_2/M_1) of SUVs with bound PZ (produced by mixing 10 μM lipid monomer with 0.47 μM PZ), where M_1 represents the molecular mass of free SUVs, as a function of added wild-type or quadruple variant ZPI. Relative changes in SUV molecular mass were calculated from changes in light scattering as described previously (18). The *solid line* is a fit of data by the quadratic binding equation. Only wild-type ZPI binds to the PZ·SUV complex and results in a saturable increase in mass.

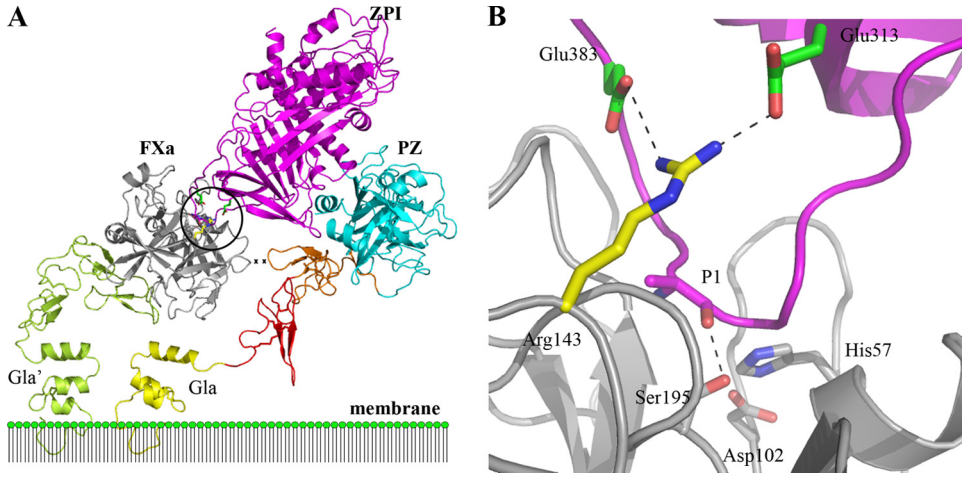

FIGURE 4. **Model of the ternary Michaelis complex of fXa with PZ-associated ZPI.** *A,* ternary complex generated from docking the structure of fXa with the present binary complex of ZPI·$PZ_{\Delta GD}$. Gla domains from a structure of factor IXa (39) have also been modeled and positioned partially embedded into the membrane and close enough to one another to interact. The area of contact between the active site of fXa and ZPI is *circled*. A putative interaction between EGF2 of PZ and the 37 loop of fXa is indicated by *asterisks*. *B,* expansion of the area *circled in A* that includes the principal contacts between fXa and ZPI. Arg-143 on fXa forms tight salt bridge interactions with Glu-383 in the RCL and Glu-313 in the body of ZPI. The RCL is positioned to allow the P1 backbone to interact with the catalytic triad of Ser-195, His-57, and Asp-102 and for the P1 side chain to project into the S1 pocket.

role for these residues in binding and in correctly orienting the ZPI relative to the proteinase. With the exception of chicken ZPI in which residue 383 is Asp, both of these residues are completely conserved in the six known sequences. In addition, the catalytic domain of fXa approached closely enough to the EGF2 region of $PZ_{\Delta GD}$ that there might be contact between side chains. In our model, the side chain of Asn-105 from $PZ_{\Delta GD}$ is close enough to contact the side chains of Glu-37 and Glu-39 of fXa (*asterisks* in Fig. 4*A*).

The other important aspect of the model of the Michaelis complex is the location and orientation of the EGF domains of fXa and protein Z with respect to one another. These are on the same "side" of the ZPI RCL and are oriented such that, were their Gla domains attached, the Gla domains would easily be able to interact with one another on the membrane surface (Fig. 4*A*). This is another important aspect of the specificity of protein Z-complexed ZPI for membrane-associated fXa, because it has been shown from Gla domain-swap variants, that such a Gla-Gla interaction contributes to specificity (6).

Importance of Glu-313 and Glu-383—To evaluate the role of each of these conserved glutamic residues, implicated by modeling the ternary Michaelis complex in binding fXa, we mutated them singly and jointly to alanine and determined the kinetic constants for inhibition of fXa and fXIa. All variant forms of ZPI inhibited fXa in a stable manner (Fig. 5). For inhibition of fXa in the presence of PZ, lipid, and Ca^{2+} cofactors, there was a 10-fold reduction in the rate constant for the E313A mutant but no effect for the E383A mutant after correcting the association rate constants for differing SIs (Table 1). The double mutant behaved the same as the E313A mutant. In the absence of PZ, only the E313A mutation resulted in a reduction in second order rate constant of about 5–10-fold. Similar results were found for the PZ-independent inhibition of fXIa, for which the E313A variant and the double variant both showed a reduction of about 10-fold in second order rate constant, whereas the E383A variant reacted like wild type (Table 2). Although residue Glu-383 did not seem to be important for formation of the Michaelis complex, it did have an effect on the subsequent partitioning between substrate and inhibitory branches of the reaction pathway, because both the single and double variants that contained the E383A mutation showed much higher SI values than wild-type ZPI or the E313A variant (Table 1).

These results clearly establish an important role for Glu-313 in promoting the rate of inhibition of both fXa and fXIa, presumably from the proposed direct interaction with the proteinase suggested by the model, but in a manner that is independent of PZ. However, Glu-383 appears not to be important for formation of the Michaelis complex but may be involved in the subsequent acylation and deacylation steps.

PZ-induced Conformational Change in ZPI—We have shown above that although Glu-313 enhances the rate of reaction between fXa and ZPI, it does not depend on PZ and is therefore not the source of the large PZ-dependent rate enhancement of inhibition of fXa by ZPI. We therefore examined other possible sources of the enhancement. One was the possibility of PZ-induced conformational changes in ZPI that make it more reactive toward fXa. To examine this, we used several solution approaches that might sense conformational change.

In the first, a P7 Cys variant (L381C) was used to introduce an NBD fluorophore in the ZPI RCL. The NBD label had minimal effect on the functional properties of ZPI, with a rate acceleration of fXa inhibition promoted by full-length PZ, lipid, and Ca^{2+} that was almost identical to that of wild-type ZPI (when corrected for an increase in SI). Even though the closest approach of $PZ_{\Delta GD}$ to this position in the complex is about 23 Å, NBD responded to PZ binding, with a 15–20% decrease in fluorescence intensity (Fig. 6*A*), suggesting that there is a conformational change sensed in the RCL. Titration of PZ into NBD-ZPI, followed by change in NBD fluorescence, gave a K_d for the interaction of 6 ± 4 nM and a 1:1 stoichiometry (Fig. 6*A*, *inset*). To show the conformational change was not the result of the presence of the Gla domain, the experiment was repeated using $PZ_{\Delta GD}$, with similar perturbation of the NBD fluorophore in the RCL (data not shown).

As a probe for conformational change in the body of the serpin, NBD was attached to an S122C variant. This residue lies at the intersection of helix D with the N-terminal end of helix A, whereas the C-terminal end of helix A is located about 32 Å away at the interface with PZ. The NBD fluorescence decreased 10–15% upon binding $PZ_{\Delta GD}$ but much less on binding intact PZ (Fig. 6*B*).

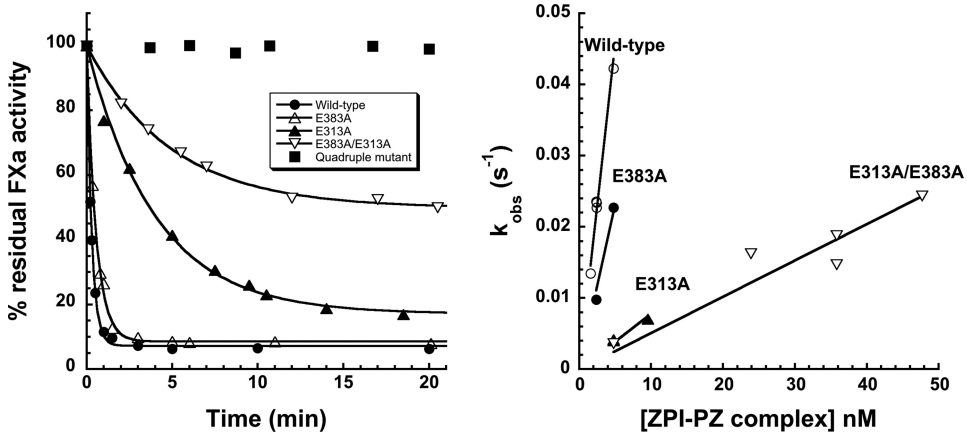

FIGURE 5. **Effect of mutating ZPI residues Glu-313 and Glu-383 on inhibitory activity.** *Left panel,* progress curves for reaction of wild-type, E313A, E383A, E313A/E383A, and quadruple variant ZPIs (40 nM) with fXa (0.1 nM) in the presence of 5 nM PZ, 25 μM lipid, and 5 mM Ca^{2+}. Percentage residual activity of fXa measured from the initial rate of hydrolysis of 50 μM Pefafluor fXa is plotted as a function of time. *Solid lines* are computer fits to a single exponential function with nonzero end point. *Right panel*, k_{obs} plotted as a function of [ZPI] for reactions of the various forms of ZPI with 0.1 nM fXa in the presence of 25 μM lipid and 5 mM Ca^{2+}. [PZ] was varied in all cases, with ZPI fixed at 20–40 nM for wild-type, E313A, and E383A variants and at 240–250 nM for the E313A/E383A variant. *Solid lines* are linear regression fits in which the ordinate intercept was fixed at the measured ZPI·fXa complex dissociation rate constant in Table 1.

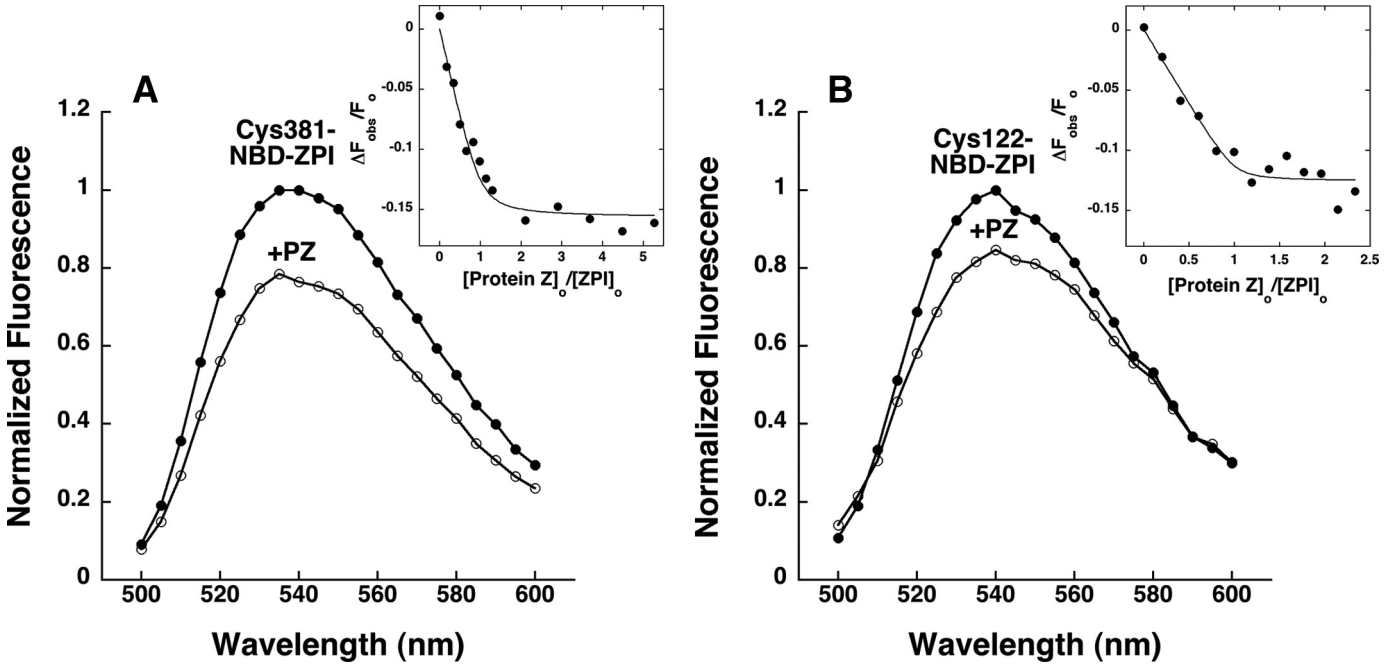

FIGURE 6. **Evidence of PZ-induced conformational change in ZPI.** *A,* normalized fluorescence of NBD attached to position 381 (P7 in the RCL) of ZPI (100 nM) in the absence (●) and presence of equimolar PZ (○). *Inset* is the fractional change in fluorescence as a function of added PZ. *B,* normalized fluorescence of NBD attached to position 122 (helix D) of ZPI (100 nM) in the absence (●) and presence of PZ (○). *Inset* is the fractional change in fluorescence as a function of added PZ.

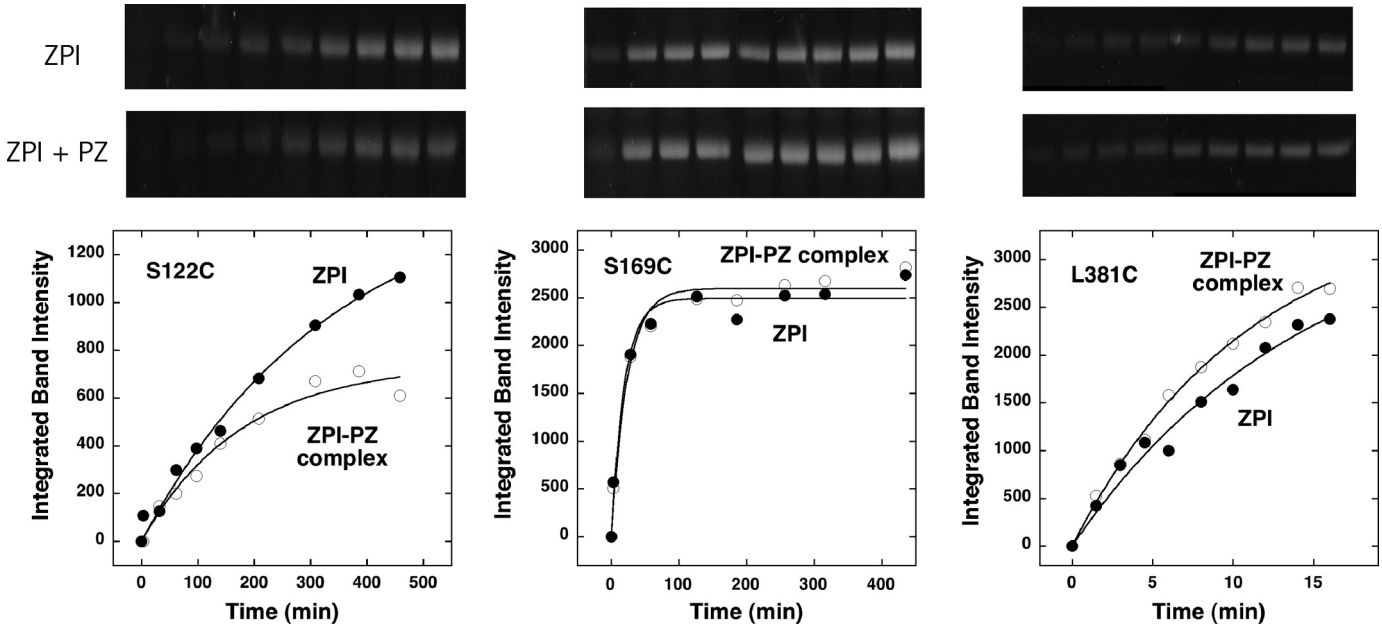

FIGURE 7. **Effect of PZ on cysteine reactivity on ZPI.** *Top panels,* photographs of fluorescein fluorescence associated with the ZPI band on SDS-PAGE in the absence (*upper gel*) and presence (*lower gel*) of PZ. The time points sampled correspond to those of the plots in the *lower panels. Lower panels,* plots of integrated band intensities of ZPI fluorescence as a function of labeling time, in the absence and presence of PZ. *Left panels,* reaction at Cys-122 (helix D); *middle panels*, reaction at Cys-169 (control on s1A); *right panels*, reaction at Cys-381 (P7 of RCL).

This suggests that binding of PZ results in transmission of perturbation via helix A to its distal N-terminal end. Titration of the fluorescence change resulted in an immeasurably tight K_D (5 ± 5 nM) and a 1:1 stoichiometry (Fig. 6*B, inset*).

A third approach to examining PZ-induced perturbation in the RCL and helix A/D crossover of ZPI used the reactivities of two ZPI cysteine variants (Cys-122 and Cys-381) toward iodoacetamidofluorescein as a function of the presence or absence of PZ. Both cysteines changed reactivity as a result of PZ binding, although Cys-381 showed a slight increase when PZ was bound (Fig. 7, *right*), whereas the reactivity of Cys-122, which was already about 2 orders of magnitude lower than for Cys-381, was reduced by ~50% upon binding of PZ (Fig. 7, *left*). To examine whether PZ induced a more global conformational rearrangement, the reactivity of a cysteine at a site at the distal end of sheet A (Cys-169) was examined (Cys-169 on s1A) but showed no effect of protein Z binding on rate of reaction (Fig. 7, *center*). Together, the three approaches suggest that binding of PZ or $PZ_{\Delta GD}$ causes structural changes in ZPI that are sensed in the RCL as well as at the distal end of helix A from its site of interaction with PZ.

Importance of Membrane Association for Reactivity—It was shown above by light scattering that ZPI only associates with the membrane surface when complexed with PZ, because of PZ possessing a membrane-binding Gla domain (Fig. 2). Comparison of the ability of full-length and Gla-domainless PZ to inhibit fXa in the presence of lipid and Ca^{2+} should therefore discriminate between PZ-induced conformational change effects and those due solely to membrane association. We found that, in the presence of lipid and Ca^{2+}, binding of $PZ_{\Delta GD}$ to ZPI resulted in only a 2-fold increase in the second order rate constant compared with the reaction in the absence of $PZ_{\Delta GD}$ (Table 3). Similarly, PZ alone, in the absence of phospholipid and Ca^{2+} gave no rate enhancement (Table 3). This suggests

TABLE 3

Effect of lipid, calcium, protein Z, and Gla domainless protein Z cofactors on the reaction of wild-type ZPI with fXa and Gla domainless fXa

I is inhibitor; E is proteinase.

Cofactors	$k_{a,app}$	SI	$k_{a,app}$ × SI
	$M^{-1}s^{-1}$	*mol I/mol E*	$M^{-1}s^{-1}$
None	$1.0 \pm 0.1 \times 10^4$	3.6 ± 0.4	$3.6 \pm 0.8 \times 10^4$
+PZ	$5.6 \pm 0.2 \times 10^3$	6.8 ± 0.1	$3.8 \pm 0.2 \times 10^4$
+Lipid	$9.7 \pm 0.4 \times 10^3$	3.2 ± 0.2	$3.1 \pm 0.3 \times 10^4$
$+Ca^{2+}$	$4.7 \pm 0.4 \times 10^3$	4.5 ± 0.2	$2.1 \pm 0.3 \times 10^4$
+Lipid + Ca^{2+}	$2.1 \pm 0.1 \times 10^3$	6.2 ± 0.1	$1.3 \pm 0.1 \times 10^4$
+Lipid + Ca^{2+} + PZ	$9.1 \pm 0.2 \times 10^6$	3.1 ± 0.2	$2.8 \pm 0.2 \times 10^7$
+Lipid + Ca^{2+} + $PZ_{\Delta GD}$	$7.3 \pm 0.3 \times 10^3$	3.8 ± 0.1	$2.8 \pm 0.2 \times 10^4$
None, $fXa_{\Delta GD}$	$6.2 \pm 0.2 \times 10^3$	3.6 ± 0.1	$2.2 \pm 0.1 \times 10^4$
+Lipid + Ca^{2+} + PZ, $fXa_{\Delta GD}$	$4.8 \pm 0.1 \times 10^3$	3.3 ± 0.1	$1.6 \pm 0.1 \times 10^4$

that conformational change in ZPI induced by PZ binding causes, at most, a 2-fold increase in the second order rate constant for inhibition of membrane-associated fXa. In contrast, the difference in second order rate constant for complexes of ZPI with full-length PZ or $PZ_{\Delta GD}$ in the presence of lipid and Ca^{2+} was 1000-fold (Table 3), suggesting that membrane association alone is the overwhelmingly dominant contributor to the PZ-induced rate enhancement. Consistent with the overwhelming contribution to rate enhancement of membrane association rather than conformational change, an 1800-fold drop in rate of inhibition was observed in the presence of lipid, Ca^{2+}, and full-length PZ when $fXa_{\Delta GD}$ was used rather than full-length fXa (Table 3).

Although the reason is not obvious, the PZ-induced conformational change in ZPI resulted in a reduction in SI of ~2-fold for the reaction of ZPI with membrane-bound fXa (from 6.2 to 3.1), whereas the same conformational change has the opposite effect on the reaction with free fXa (from 3.6 to 6.8) (Table 3).

Significance of the P1 Tyrosine—The above results show that, even though PZ causes some conformational changes in ZPI, it brings about almost all of the acceleration of the reaction of ZPI

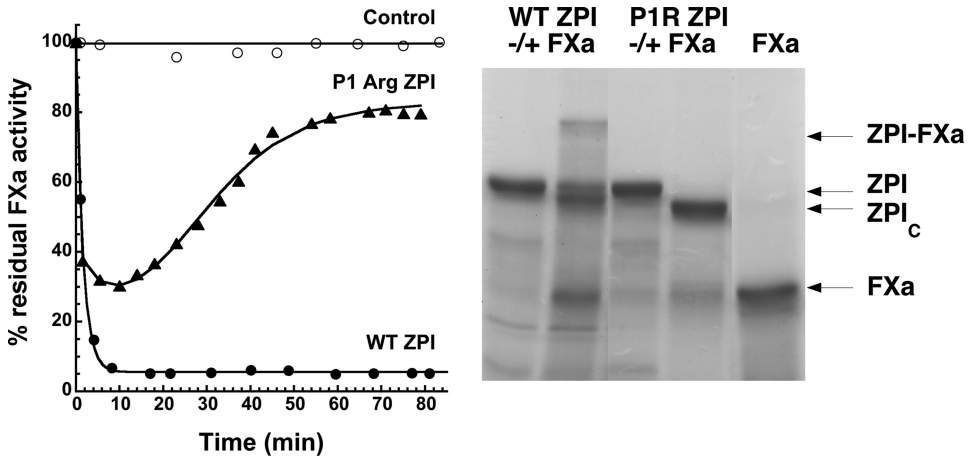

FIGURE 8. **Formation and rapid decay of P1 Arg ZPI·fXa complexes.** *Left panel*, progress curves for inhibition of 5 nM fXa by 1 μM wild-type or P1 Arg ZPIs in the absence of PZ, lipid, and Ca^{2+} cofactors. The U-shaped curve for the P1 Arg ZPI reaction reflects the formation and rapid deacylation of the covalent complex formed between fXa and P1 Arg ZPI. *Solid lines* are fits of the wild-type reaction to a single exponential function and of the P1 Arg ZPI reaction by numerical integration of the differential equations for the acylation and deacylation phases of the serpin-proteinase reaction (9). *Right panel*, SDS-PAGE of the reaction of 3 μM wild-type ZPI with fXa at a 2:1 ratio of serpin/proteinase and of 3 μM P1 Arg ZPI reaction with fXa at a 50:1 ratio of serpin/proteinase, carried out in the absence of cofactors for ~2–3 min. Reactions were quenched with SDS at acid pH to observe complex formation. Note that a covalent ZPI·fXa complex is observed only for the wild-type reaction because of the predominant formation of cleaved ZPI (ZPI_c) in the reaction of P1 Arg ZPI. Moreover, the wild-type reaction is incomplete over the time frame that the P1 Arg reaction is complete using catalytic levels of fXa.

with fXa by localizing the ZPI, through its complex with PZ, to the membrane surface. If a high rate of reaction for membrane-bound fXa thus results predominantly from membrane association, why then does ZPI have a P1 tyrosine? To address this question, we examined the properties of a P1 Arg variant of ZPI. Even in the absence of cofactors, the P1 Arg ZPI reacted with fXa with a second order rate constant of 1.2×10^7 M^{-1} s^{-1} (Table 1). This is about 300-fold faster than wild-type ZPI. Given that this rate constant approaches a diffusion-limited value, it was not surprising that PZ, phospholipid, and Ca^{2+} gave only ~4-fold additional enhancement (Table 1). Similar rapid rate of reaction was found with fXIa, although the second order rate constant increased only modestly compared with the already rapid reaction of wild-type ZPI (Table 2).

Surprisingly, each of these reactions with the P1 Arg variant had a very high SI, ranging from ~400 with fXa to ~1000 with fXIa, compared with values of 3.1–8 for reactions with wild-type ZPI. The consequence of this is that most ZPI ends up as cleaved, inactivated serpin, rather than as covalent complex when reacted with either fXa or fXIa (Fig. 8, *right panel*). Also of note is that the rate at which the covalent complex deacylates, which is a measure of how much residual catalytic activity remains in the normally quite inactive covalent acyl enzyme complex, is 17–35 times higher for P1 Arg variant than for wild-type ZPI with fXa or fXIa respectively (Tables 1 and 2). This may be a consequence either of less effective inactivation of the catalytic triad in the distorted covalent complex or else an intrinsically higher catalytic rate than wild type, which leaves a higher residual activity upon distortion. The consequence of such relatively rapid deacylation under physiological conditions is that the time dependence of residual activity shows a distorted U-shaped profile, with initial inactivation, as complex is formed, followed by recovery of activity as the complex is hydrolyzed and active proteinase is released (Fig. 8). Numerical fitting of this U-shaped progress curve to the differential equations for the serpin inhibition mechanism suggests that the measured SIs, and hence the corrected second order inhibition rate constants in Tables 1 and 2, may be overestimated by a factor of 2–3 because of the instability of the complexes.

DISCUSSION

We have shown that PZ forms a tight complex with ZPI at a site involving helix G and the C-terminal end of helix A, which is well removed from the reactive center loop. This site is quite different from any other known site of interaction between a serpin and cofactor. Through the Gla domain of PZ, this targets the PZ·ZPI complex to the membrane surface, although ZPI is held well above the membrane surface and does not interact with it through any part of the serpin. Although a highly conserved glutamic acid in ZPI, Glu-313, engages fXa in the ternary Michaelis complex and contributes about 10-fold to the overall second order rate constant for inhibition, it does so in a PZ-independent way and so does not contribute to the PZ-dependent rate enhancement of the reaction. Instead, membrane association, *per se*, seems to be by far the dominant factor in the enhancement. This is made up of two components. One is a specific interaction between the Gla domains of fXa and PZ that was previously identified by Rezaie and co-workers (6) and that contributes ~6-fold to the rate enhancement. However, this leaves up to 400-fold of the rate enhancement to the template effect of the membrane in bridging between PZ·ZPI and fXa, thereby bringing together the RCL of the ZPI and the active site of fXa in a much more efficient manner.

Although it was expected that a P1 Arg variant of ZPI would react more rapidly with fXa than did wild-type ZPI (>300-fold faster in the absence of PZ), it was a surprise both that the reaction was predominantly as a substrate, reflected in very high SI values, and that the complex that was trapped by the normal serpin mechanism dissociated rapidly. This was also true for the reaction with fXIa. The predominant substrate reactions do not, however, imply a different mechanism of reaction from that normally found with serpins, but rather that partitioning of the acyl intermediate between the branches of the pathway that lead to cleaved ZPI and trapped complex strongly favor the former. Because the mutation is at P1, which does not even become part of β-sheet A in the covalent complex (29), the change in partitioning is unlikely to result from a change in rate of the insertion of the RCL into the sheet. Instead, it is likely to result from a much more rapid deacylation of the acyl enzyme intermediate, perhaps as a result of better

accommodation of the P1 residue in the S1 pocket of the proteinase, whether fXa or fXIa, when the P1 is arginine rather than tyrosine. This in turn may also account for the lower stability, in the case of the P1 Arg ZPI, of the covalent complex that does form. Thus, it has been found for other serpins that the P1 side chain alters its positioning in the S1 pocket in the trapped acyl enzyme intermediate (30). For the better fitting arginine, this may still result in greater residual catalytic activity in the distorted ZPI·proteinase complex than for the tyrosine. However, it should be noted for the P1 arginine that the rate of deacylation is 4 orders of magnitude faster than for the same proteinase, fXa, with a different serpin, antithrombin (31), implying that ZPI is less effective at inactivating the catalytic machinery of the proteinase in the distorted serpin·proteinase complexes. The P1 tyrosine of ZPI, together with the conserved Glu-383 at position P5, thus appear to play an important role in ensuring that ZPI reacts as an inhibitor rather than a substrate with either fXa or fXIa and that the resulting covalent complexes are reasonably stable.

It should also be realized that the rate of reaction with fXa of the P1 Arg ZPI variant in the absence of PZ is about 1000-fold faster than for antithrombin. This is despite the two serpins having very similar sequences for residues P4–P1′ of ITARS and IEGRS, respectively. Even the effects of differences are either neutral (Thr for Glu at P3) or favor antithrombin over ZPI (Gly is preferred over Ala 5-fold at P2) in peptide substrates (32). Taking these preferences into account and eliminating the 5-fold increase in rate for the ZPI reaction that results from the interaction with Glu-313 leaves relative rates of about 1000:1 for ZPI compared with antithrombin (decrease of 5-fold for Glu-313 and increase of 5-fold for Ala-to-Gly difference). This reinforces an earlier conclusion that antithrombin, in the absence of cofactor, represents a repressed conformational state that is de-repressed only when cofactor is present (33). In the case of ZPI the repression of rate in the absence of cofactor results from the P1 tyrosine. This is overcome by template bridging and consequent Gla domain interaction in the presence of PZ, phospholipid, and Ca^{2+} and to a minor extent by PZ-induced conformational change in ZPI.

The advantage of such a mechanism, in which an unfavorable P1 residue (Tyr) is used to produce a low rate of reaction in the absence of cofactors that is offset by the favorable interactions resulting from association with PZ and the lipid surface, is to ensure that ZPI can only inhibit fXa when the latter is associated with the platelet membrane, as it would be immediately after its generation from the Xase complex. Although the overall rate of reaction would be higher if the P1 residue of ZPI were an Arg, this would come at the expense of eliminating the membrane localization specificity that is presumably the raison d'être of ZPI, as well as turning ZPI into an ineffectual substrate. The ZPI-protein Z system is thus yet another example of how serpins achieve specificity by having suppressed rates of reaction, unless and until auxiliary factors are provided (34). A somewhat parallel example of achieving specificity for fXa inhibition over other arginine-specific proteinases is provided by an inhibitor of a different class, TAP. TAP also has a P1 tyrosine but overcomes the resulting low affinity interaction by dominant exosite interactions involving the N terminus of the inhibitor (35, 36).

Interestingly, the high reactivity of ZPI with fXIa ($\sim 10^6\ M^{-1}\ s^{-1}$), which is also independent of cofactors, is mediated in part by the same Glu-313 exosite in strand 2C that contributes to the reactivity with fXa. As with fXa, Glu-313 presumably interacts with basic residues in the 140 loop of fXIa that have been implicated in ZPI reactivity with this proteinase (37). Also of note, wild-type ZPI, with P1 tyrosine, is only marginally less reactive with fXIa than the P1 arginine variant, although the tyrosine does ensure that the ZPI is a better inhibitor (much lower SI). The SI is further lowered in the presence of the fXIa cofactor heparin (9).

A final notable aspect of the system is that upon insertion of the RCL into β-sheet A, whether to form cleaved or proteinase-complexed ZPI, the affinity for the PZ cofactor drops by several orders of magnitude (9) and results in the effective release of the cofactor, which consequently behaves in a catalytic fashion. This raises the question of how such modulation of the affinity of the complex comes about, because the contact interface involves neither the RCL nor the surface of β-sheet A. Here, it may be significant that two of the charged residues on ZPI that are involved with interface interactions occur on helix A (Lys-68 and Asp-74). We showed above that PZ binding to ZPI results in some long range conformational change, including perturbations at the distal end of helix A from the interface with PZ. Although the extremely long helix A does not lie in direct contact with the underside of β-sheet A, it does contact helices B and D, which do contact the sheet. Thus, sheet expansion that results from RCL insertion may indirectly perturb the positioning of helix A and may cause disruption of the interface with PZ by altering the location and/or orientation of Lys-68 and Asp-74.

Such a linkage between the PZ:ZPI interface and helix A suggests a possible role for the extreme N terminus that precedes helix A and that is not ordered sufficiently to be seen in the x-ray structure of the complex. It is possible that interactions of this region with other proteins may also modify the position of helix A and so influence the ability of ZPI to bind tightly to PZ and so to inhibit fXa.

Acknowledgments—We thank Dr. George Broze, Jr. for providing the cDNA for human ZPI and Dr. Ray Rezaie for providing recombinant Gla-domainless fXa.

REFERENCES

1. Davie, E. W., Fujikawa, K., and Kisiel, W. (1991) *Biochemistry* **30,** 10363–10370
2. Olson, S. T., and Björk, I. (1994) *Persp. Drug Discov. Design* **1,** 479–501
3. Han, X., Fiehler, R., and Broze, G. J., Jr. (1998) *Proc. Natl. Acad. Sci. U.S.A.* **95,** 9250–9255
4. Han, X., Huang, Z. F., Fiehler, R., and Broze, G. J., Jr. (1999) *Biochemistry* **38,** 11073–11078
5. Han, X., Fiehler, R., and Broze, G. J., Jr. (2000) *Blood* **96,** 3049–3055
6. Rezaie, A. R., Bae, J. S., Manithody, C., Qureshi, S. H., and Yang, L. (2008) *J. Biol. Chem.* **283,** 19922–19926
7. Ngai, P. K., and Chang, J. Y. (1991) *Biochem. J.* **280,** 805–808
8. Rezaie, A. R. (2000) *J. Biol. Chem.* **275,** 3320–3327
9. Huang, X., Swanson, R., Broze, G. J., Jr., and Olson, S. T. (2008) *J. Biol.*

Chem. **283,** 29770–29783
10. Gill, S. C., and von Hippel, P. H. (1989) *Arch. Biochem. Biophys.* **182,** 319–326
11. Broze, G. J., Jr., and Miletich, J. P. (1984) *J. Clin. Invest.* **73,** 933–938
12. McCoy, A. J. (2007) *Acta Crystallogr. D Biol. Crystallogr.* **63,** 32–41
13. Murshudov, G. N., Vagin, A. A., and Dodson, E. J. (1997) *Acta Crystallogr. D Biol. Crystallogr.* **53,** 240–255
14. Heeb, M. J., Mesters, R. M., Tans, G., Rosing, J., and Griffin, J. H. (1993) *J. Biol. Chem.* **268,** 2872–2877
15. Anderson, P. J., Nesset, A., Dharmawardana, K. R., and Bock, P. E. (2000) *J. Biol. Chem.* **275,** 16435–16442
16. Stewart, J. C. (1980) *Anal. Biochem.* **104,** 10–14
17. McDonald, J. F., Shah, A. M., Schwalbe, R. A., Kisiel, W., Dahlbäck, B., and Nelsestuen, G. L. (1997) *Biochemistry* **36,** 5120–5127
18. Nelsestuen, G. L., and Lim, T. K. (1977) *Biochemistry* **16,** 4164–4171
19. Olson, S. T., Swanson, R., Raub-Segall, E., Bedsted, T., Sadri, M., Petitou, M., Hérault, J. P., Herbert, J. M., and Björk, I. (2004) *Thromb. Haemost.* **92,** 929–939
20. Hood, D. B., Huntington, J. A., and Gettins, P. G. (1994) *Biochemistry* **33,** 8538–8547
21. Swanson, R., Raghavendra, M. P., Zhang, W., Froelich, C., Gettins, P. G., and Olson, S. T. (2007) *J. Biol. Chem.* **282,** 2305–2313
22. Huntington, J. A., and Gettins, P. G. (1998) *Biochemistry* **37,** 3272–3277
23. Wei, Z., Yan, Y., Carrell, R. W., and Zhou, A. (2009) *Blood* **114,** 3662–3667
24. Gettins, P. G. (2002) *Chem. Rev.* **102,** 4751–4804
25. Chandrasekaran, V., Lee, C. J., Duke, R. E., Perera, L., and Pedersen, L. G. (2008) *Protein Sci.* **17,** 1354–1361
26. Ichinose, A., Takeya, H., Espling, E., Iwanaga, S., Kisiel, W., and Davie, E. W. (1990) *Biochem. Biophys. Res. Commun.* **172,** 1139–1144
27. Lee, C. J., Chandrasekaran, V., Duke, R. E., Perera, L., and Pedersen, L. G. (2007) *J. Thromb. Haemost.* **5,** 1558–1561
28. Rezaie, A. R., Manithody, C., and Yang, L. (2005) *J. Biol. Chem.* **280,** 32722–32728
29. Dementiev, A., Dobó, J., and Gettins, P. G. (2006) *J. Biol. Chem.* **281,** 3452–3457
30. Futamura, A., Stratikos, E., Olson, S. T., and Gettins, P. G. (1998) *Biochemistry* **37,** 13110–13119
31. Calugaru, S. V., Swanson, R., and Olson, S. T. (2001) *J. Biol. Chem.* **276,** 32446–32455
32. Bianchini, E. P., Louvain, V. B., Marque, P. E., Juliano, M. A., Juliano, L., and Le Bonniec, B. F. (2002) *J. Biol. Chem.* **277,** 20527–20534
33. Gettins, P. G., and Olson, S. T. (2009) *FEBS Lett.* **583,** 3397–3400
34. Gettins, P. G., and Olson, S. T. (2009) *J. Biol. Chem.* **284,** 20441–20445
35. Jordan, S. P., Mao, S. S., Lewis, S. D., and Shafer, J. A. (1992) *Biochemistry* **31,** 5374–5380
36. Wei, A., Alexander, R. S., Duke, J., Ross, H., Rosenfeld, S. A., and Chang, C. H. (1998) *J. Mol. Biol.* **283,** 147–154
37. Rezaie, A. R., Sun, M. F., and Gailani, D. (2006) *Biochemistry* **45,** 9427–9433
38. Schechter, I., and Berger, A. (1967) *Biochem. Biophys. Res. Commun.* **27,** 157–162
39. Brandstetter, H., Bauer, M., Huber, R., Lollar, P., and Bode, W. (1995) *Proc. Natl. Acad. Sci. U.S.A.* **92,** 9796–9800